International Journal of Research
Available at https://edupediapublications.org/journals
e-ISSN: 2348-6848
p-ISSN: 2348-795X
Volume 04 Issue 13
October 2017

Study of Mineralogical diversity and Scattering characteristics of Lunar Equatorial region using Chandrayaan-1 data

Manish Sharma[1], S. Arivazhagan[2] and A. Karthi[2]

1-University of Petroleum and Energy Studies, Dehradun-248007, Uttarakhand, India

2-Gandhigram Rural Institute- Deemed University, Gandhigram, Dindigul-624302,Tamil Nadu, India

Corresponding Author Email id: sharma.m2225@gmail.com

ABSTRACT

Mineral mapping of lunar surface is significant to understand the origin, evolution, geological history of the Moon. Advancements in orbital satellite sensor technology has allowed discriminating the minerals on lunar surface using hyperspectral data. Moon Mineralogy Mapper (M^3) is an imaging spectrometer that has provided the first high-resolution spatial and spectral map of the entire lunar surface. Band ratio and spectral profiling methods are used for identifying minerals. 1 µm and 2 µm band depth derived from Moon Mineralogy Mapper data were used to detect the Olivine and Calcic-Pyroxene rich sites. Mini-SAR of Chandrayaan-1 is the very first kind of hybrid polarimetric radar flown outside the Earth's orbit. The hybrid polarimetric architecture of mini-SAR allows the measurement of the Stokes parameters and backscatter properties of various lunar geological features. SAR is a powerful tool to study the physical and geometrical properties of lunar morphological features and the magnitude and characteristics of SAR backscatter and m-χ decomposition parameters are critical in understanding the morphology and nature of deposits associated with lunar surface features. In this paper Mineralogical diversity and Scattering characteristic of Byrgius Crater, King Crater, Maunder Crater, Taylor Crater and Descartes Crater were investigated using Chandrayaan-1 data.

Keywords: Chandrayaan-1, Hyperspectral, Moon Mineralogy Mapper, Mini-SAR, Band depth.

1. Introduction:

The Moon has been explored using several unmanned and manned missions between 1960's and 1990's. These explorations have yielded valuable information on the physical and chemical properties of the Moon. The study of the mineral composition can provide information on a record of the thermal and chemical evolution of a planetary body because various processes like differentiation and volcanism produce distinct mineral signatures. Therefore, the mineralogical composition studies are known as powerful tools for unravelling the geologic history of a planetary body. Advancements in orbital satellite technology have allowed the evaluation of surface lithology of the Moon through mineralogical mapping using high spectral and spatial resolution data (e.g. SELENE Spectral Profiler, Multi-band Imager and Moon Mineralogy Mapper (M^3)) (V. Siva, et al., 2017). The M^3 on-board Chandrayaan-1, the Indian Space Research Organisation's (ISRO) first mission to the Moon (Goswami, et al., 2009) provides information about the lunar surface mineralogy. The reflectance data of the Moon Mineralogy Mapper (M^3) are used to study the composition on the lunar surface. M^3 is a hyper spectral imager with the best spatial resolution (140 m/pixel or 280 m/pixel) and spectral range available, with 85 spectral channels spanning from 430 to 3000 nm (Mohan, et al., 2011) allowing for optimal accuracy in determining surface mineralogy. The band shape algorithms such as standard band ratio, 1 µm and 2 µm band depths is used for lunar surface mineralogy.

A comprehensive study and comparison of different morphological features can have significant implications for the compositional stratigraphy of the lunar crust which could provide clues to the thermal history and chemical evolution of the Lunar. Synthetic Aperture Radar (SAR) is a powerful remote sensing tool for studying planetary surfaces and subsurface due to the sensitivity of radar signal to the roughness, structure and composition of the surface material and its

ability to penetrate the surface to reveal the buried terrain (Carter, et al., 2011).

Mini- SAR data is primarily used to identify signatures suggesting the possibility of the presence of water ice (Fa, et al., 2013). Further, this data has been used to view various other geological features such as melt flows, crater ejecta blankets, secondary craters etc. (Saran, et al., 2012). Therefore, identification of distinct morphological features in shadowed as well as illuminated regions of lunar surfaces can be easily done using mini-SAR data (Spudis, et al., 2014). Digital image processing of mini-SAR data using m-χ decomposition technique was done to achieve single, double, and multiple/diffuse back scattering contributions to view tectonically derived morphological features in detail (Saran, et al., 2012). In the present study we are focussing on Mineralogical diversity and scattering characteristics of Byrgius Crater, King Crater, Taylor Crater, Descartes Crater and Maunder Crater.

2. Study area

Figure 1 provides the details of the lunar features studied using Moon Mineralogy Mapper (M^3) and Mini-SAR data. Among these features, the King, Byrgius, Taylor and Descartes craters belong to the lunar highland region, while the Maunder craters is part of the Mare Orientale basin on the lunar near side. The Study area of craters on lunar map is shown in figure 1.

2.1 King Crater - King is a prominent lunar impact crater that is located on the far side of the Moon, and cannot be viewed directly from Earth. To the northwest is the crater Lobachevskiy and Guyot is located an equal distance to the north-northwest.

2.2 Byrgius Crater- Byrgius is a lunar crater located in the western part of the Moon, near the limb. As a result, Byrgius appears strongly oval in form due to foreshortening. To the northwest is the nearly ruined crater Lemarch.

2.3 Maunder Crater- Maunder is a lunar impact crater that is located on the far side of the Moon, just beyond the western limb.

The crater lies at the northern end of the Mare Orientale, within the ring of mountains named Montes Rook, and it is the largest crater on this lunar mare. To the southeast is the crater Kopff, and due south is the small Hohmann.

2.4 Taylor Crater - Taylor is a lunar crater that is located to the south-southwest of Delambre. To the east is the smaller crater Alfraganus, and southeast of Taylor is Zollner.

2.5 Descartes Crater- Descartes is a heavily worn lunar crater that is located in the rugged south-central highlands of the Mon. To the southwest is the crater Abulfeda.

3. Methods and Materials:

The India's maiden planetary mission to the Moon Chandrayaan-1 was launched on October 22nd, 2008. It carried 11 payloads. The First Indian precious lunar mission Chandrayaan-1 Moon Mineralogical Mapper (M^3) and mini-SAR data were used for this study. M^3 is a push broom imaging spectrometer operating in the wavelength range of 0.43 to 3.0 µm (Pieters, 2009b). The data was recorded in two modes, a target mode with 260 spectral bands and 70 m/pixel spatial resolution, and a global mode with 85 spectral bands and 140 m/pixel spatial resolution and 40 km swath for images. Here we are using M^3 data in target mode with 85 spectral bands.

Mini-SAR was designed to image only the lunar polar regions but it also collected few strips of images at an incidence angle of ~35° over lunar equatorial and low latitude regions (Saran, et al., 2012). The data used in this project is hybrid polarimetric data from Chandrayaan-1 mini-SAR. This was obtained in SAR mode and was formatted and stored in a planetary data system (PDS) compliant standards. The data product is comprised of four channels of data, Horizontal ($|LH^2|$) and the Vertical ($|LV^2|$) channels of the dual-polarized receiver, the Real (LH.LV*) and Imaginary (LH.LV*) cross-product of the complex H and V amplitudes.

The data product was acquired in baseline SAR mode, the sensor operated in the S-band (wavelength 12.6 cm), with an incidence angle of 35º, and a ground range resolution of 150 m. The Moon Mineralogical Mapper (M^3) and Mini-SAR data is obtained from the NASA PDS geosciences node.

4. Moon Mineralogical Mapper M^3 Data Products and Analysis Strategy

4.1 Standard band ratio and Spectral Profile analysis

The band shape algorithms such as standard band ratio are employed at crucial wavelengths to delineate the abundance of minerals such as olivine, low-Ca pyroxene, high-Ca pyroxene and plagioclase on the lunar surfaces. In the present study, the standard band ratio generated to discriminate the lithology of King Crater, Byrgius Crater, Maunder Crater, Taylor Crater and Descartes Crater. Based on that spectral profiles have drawn and the absorption features were characterized and spatial distribution of different rock types were estimated. The ENVI image processing software is used for deriving spectral profiles and continuum removal of sampled spectra. In the present study, the standard band ratio is carried out using the band combination of Red=750/ 540 nm, Green=750/950 nm and Blue= 540/750 nm (Arivazhagan, et al., 2012). According to (Arivazhagan, et al., 2012) in lunar highland craters, these images shows red colour indicates mature highland materials, bright blue regions indicates immature highland lithology. Spectral reflectance observations by the Moon Mineralogy Mapper (M^3) showed spectral absorptions in the range of 2.8 µm-3.0 µm indicate the presence of OH and HOH molecules, respectively (Kramer, et al., 2016). In the present study the King, Byrgius, Taylor and Descartes craters belong to the lunar highland region, while the Maunder craters are part of the Mare Orientale basin on the lunar near side.

The standard band ratio and spectral analysis of the craters are as follows-

4.1.1 Byrgius Crater- The dark yellow and orange colours in the standard band ratio image indicate the mafic units. The continuum removed spectra of Fresh/ immature highland materials are showing absorption feature nearly 930 nm, 1390nm and1940 nm indicating Ortho pyroxene and plagioclase composition. The continuum removed spectra of mafic units are showing broad absorption at 970nm and 2060nm indicate the high calcic pyroxene and 1350 nm absorption due to plagioclase. The Standard band ratio of Byrgius Crater (A) and continuum removed spectra showing different lithology in Byrgius Crater (B) is shown in figure 2.

4.1.2 King Crater-

The continuum removed spectra of Fresh/ immature highland materials are showing absorption feature nearly 930 nm, 1349 nm and 2097 nm indicating Ortho pyroxene and plagioclase composition. The continuum removed spectra of mafic units are showing broad absorption at 970 nm and 2137 nm indicate the high calcic pyroxene. Immature highland lithology represents by blue continuum removed spectra has absorptions at 989 nm and 2057 nm which is indicating the Ortho pyroxene. The continuum removed spectra of mature highland and Immature highland lithology also showing the absorption feature nearly 2860nm, indicating presence of water/ice molecules on the crater (Nozette, et al., 2001). The Standard band ratio of King Crater (A) and continuum removed spectra showing different lithology in King Crater (B) is shown in figure 3.

4.1.3 Taylor Crater –

The continuum removed spectra of Fresh/ immature highland materials are showing broad absorption at 1369 nm absorption due to plagioclase. Immature highland lithology represents by blue continuum removed spectra has absorptions at 850 nm and 1938 nm which is indicating the low calcic pyroxene.

The dark yellow colour indicates the mafic lithology. The continuum removed spectra has broad absorptions at 990 nm, and 1740 nm indicate the presence of high calcic pyroxene. The Standard band ratio of Taylor Crater (A) and continuum removed spectra showing different lithology in Taylor Crater (B) is shown in figure 4.

4.1.4 Descartes Crater-

The continuum removed spectra of Fresh/ immature highland materials are showing absorption feature nearly 910 nm and 1820 nm indicating Ortho pyroxene. The continuum removed spectra of mafic units are showing broad absorption at 1008 nm and 1805 nm indicate the high calcic pyroxene. Immature highland lithology represents by blue continuum removed spectra has absorptions at 850 nm and 1898 nm which is indicating the Ortho pyroxene. The Standard band ratio of Descartes Crater (A) and continuum removed spectra showing different lithology in Descartes Crater (B) is shown in figure 5.

4.1.5 Maunder Crater –

Maunder Crater is the largest crater on the lunar mare. The crater lies at the northern end of the Mare Orientale, within the ring of mountains named Montes Rook. In the (M^3) composite image, the yellow/orange colours indicate pyroxene-rich lithology, blue indicates crystalline plagioclase, and white (small fresh craters, mostly on the SW side) indicates olivine-rich (Spudis, et al., 2014) . The continuum removed spectra of orange colour is showing a broad absorption feature nearly 970 nm and 2177 nm indicating pyroxene while the continuum removed spectra of blue colour is showing a broad absorption at 790nm and 1489 nm indicating crystalline plagioclase. The continuum removed spectra of dark yellow colour is showing a broad absorption at 1050 nm indicating presence of Olivine.

The Standard band ratio of Maunder Crater (A) and continuum

removed spectra showing different lithology in Maunder Crater (B) is shown in figure 6.

4.2 Mapping of 1µm and 2µm band depth

Mineral composition is perhaps one of the most important considerations in predicting relative absorption band strengths. A series of mineral indicator parameters have been developed by the M^3 team as a guide to analyses and to provide products that capture the fundamental mineralogical properties of the surface. The parameters were developed to capture the dominant modes of spectral variance related to mafic silicates, soil maturity, and space weathering. Initial analyses have shown two parameters that summarize the integrated band depth of the crystal field absorptions at 1 µm and 2 µm provide an excellent summary of the mineral diversity of the lunar surface with M^3 data. (Mustard, et al., 2011). The 1 µm is indicating the Olivine abundance whereas the 2 µm is indicating the calcic-pyroxene rich sites. The 1 µm band depth has been processed with the 789 nm to 1308 nm range bands in the 20 nm interval and the 2 µm band depth measured from 1658 nm to 2457 nm range bands in the 40 nm interval (Isaacson, et al.). The algorithm for determining the integrated band depths for the 1 and 2 µm bands are given by (Mustard, et al., 2011) that are as follows-

$$\textbf{1 µm band depth} = \sum_{n=0}^{26} 1 - \frac{R(789+20n)}{RC(789+20n)}$$

$$\textbf{2 µm band depth} = \sum_{n=0}^{21} 1 - \frac{R(1658+40n)}{Rc(1658+40n)}$$

where R refers to the reflectance at a given wavelength, Rc is the continuum reflectance defined as a straight line across the absorption band, 789 and 1658 are the first wavelengths, in nanometres in a series to be integrated over, 20 and 40 specifies the wavelength interval in nanometres, and

n is the number of channels to be integrated over.

4.2.1 Byrgius Crater-

The figure 7 (A) showing the integrated band depth of 1 µm indicating the darker red sites are high concentration of olivine and pyroxene minerals absorptions. The darker black colour is low concentration of olivine, pyroxene and olivine-pyroxene mixture minerals absorptions. 2 µm integrated band depth as seen in figure 7 (B) is showing the low concentration of pyroxene present in darker black sites and high concentration of pyroxene present in the red sites, as these can be seen easily by the scale mentioned.

4.2.2 King Crater- The high and low concentration olivine, pyroxene and olivine-pyroxene mixture minerals absorptions can be seen in figure 8 (A) and 8 (B) derived by using 1 µm and 2 µm band depths of King crater.

4.2.3 Taylor Crater-The 1 µm and 2 µm band depth result of Taylor crater are shown in figure 9 (A) and 9 (B). The concentration of pyroxene and olivine presence is indicated by the given scale.

4.2.4Descartes Crater- The 1 µm and 2 µm band depth result of Descartes crater are shown in figure 10 (A) and 10 (B). The concentration of pyroxene and olivine presence is indicated by the given scale.

4.2.5 Maunder Crater-The 1 µm and 2 µm band depth result of Maunder crater are shown in figure 11 (A) and 11 (B). The concentration of pyroxene and olivine presence is indicated by the given scale.

5. Mini-SAR Data products and analysis strategy

The Mini-SAR instrument was a small, low mass, S-band (2380 MHz, 12.6 cm wavelength) imaging radar with unique

hybrid polarimetry architecture (Raney, 2007) on board Indian Chandrayaan-1 mission that was launched on October 22, 2008 (Goswami, et al., 2009). This radar transmitted in Left Circular Polarization (LCP) and received coherently in horizontal (H) and vertical (V) polarizations. A typical Mini-SAR image strip contains 16 bytes of data in four channels of 4 bytes per each pixel, where the first two channels represent the intensity images for horizontal and vertical receive and the last two represent real and imaginary components of the complex cross power intensity between the horizontal and vertical receive given by $|LH|^2$, $|LV|^2$, Real (LH LV*) and Imaginary (LHLV*) respectively (Mohan, et al., 2011). From the available data, the Stokes parameter can be computed form where parameters like circular polarization ratio (CPR), relative phase(δ) and m (Degree of polarization)–χ (Poincare ellipticity) decomposition technique can be studied. The methodology adopted to achieve the objective of the study is shown in figure 12.

5.1 Derivation of Stokes parameters

The process starts with the derivation of the Stokes parameters from the data from which follow other parameters like degree of polarization (m), relative phase (δ), Poincare ellipticity parameter (χ), CPR etc., which are used in the decomposition methods can be derived.

Stokes vector can be derived be the given equation- (Raney, 2007).

$$\begin{pmatrix} S0 &= & <|E_{LH}|^2 + |E_{LV}|^2> \\ S1 &= & <|E_{LH}|^2 - |E_{LV}|^2> \\ S2 &= & 2Re<E_{LH}.E^*_{LV}> \\ S3 &= & -2Im<E_{LH}.E^*_{LV}> \end{pmatrix} \quad (1)$$

Where 'E_{LH}' and 'E_{LV}' are the electric fields for the horizontal and vertical linear polarizations received respectively and '*' represents the conjugate of the complex number. The first subscript denotes the transmit polarization, and the second

subscript indicates the receive polarization. The sign on S3 is negative, which is consistent with the back-scattering alignment (BSA) convention (Raney, 2007). Before doing any further analysis and using band3 and band 4 for deriving stokes parameter, a phase calibration method should be applied to remove phase shift. The un-calibrated data will result into false CPR calculation. Following equation can be used for calibration of third and fourth Stokes Vector using the original data

Re (LH LV*)calib = Re (LH LV*) cos 45º - Im (LH LV*) sin 45º **(2)**

Im (LH LV*)calib = Re (LH LV*) sin 45º + Im (LH LV*) cos 45º **(3)**

5.2 The m, δ, m-χ decompositions and CPR

5.2.1 Circular polarization ratio (CPR)

The Circular polarization ratio (CPR) is the most important parameter, as it provides the indications for wavelength-scale complexity of the surface (Nozette, et al., 2001). When an incident beam reflects off a surface, it changes the sense of polarization opposite of the signal transmitted (OC). Likewise, if the beam reflects off two objects, it reverses polarization twice, therefore resulting in the same sense in which it was transmitted (SC). The CPR analysis over selected craters shows how the variations of the different parameters affect the CPR ratio, indicating reasons for the variations in the observed data. Rough, rocky surface causes incident radar beams to bounce more than once, leading to more SC signals and thus high CPR. CPR is defined as the ratio of received power in the same sense (SC) transmitted to the opposite sense (OC) (Saran, et al., 2012).The CPR can be calculated by the following formulation as given in equation (4) by (Saran, et al., 2012)

$$\textbf{Circular Polarization Ratio}(CPR) = \frac{SC}{OC} = \frac{S0-S3}{S0+S3} \quad (4)$$

5.2.2 Degree of Polarization (m)

Degree of Polarization (m) is defined as the ratio of polarized power to the total power of the electromagnetic wave. This parameter is a significant distinguisher for characterizing the polarity of the backscatter. Polarity refers to the case of fully polarized, partially polarized or completely depolarized cases. The value of m is always between 0 and 1. Random or depolarized backscatter has a degree of polarization closer to the value of 0 while for polarized backscatter the value is closer to 1, Therefore, the value of degree of polarization for surface and double bounce scattering. The Degree of Polarization (m) can be calculated by the following formulation as given in equation (5) by (Saran, et al., 2012)

$$\textbf{Degree of Polarization}\ (m) = \frac{\sqrt{S1^2+S2^2+S3^2}}{S0} \quad (5)$$

5.2.3 Relative phase (δ)

Relative phase (δ) is the angular difference of the phase between the two components of the electric field vector. δ is an indicator of double bounce scattering. The Relative phase (δ) can be calcualated by the following formulation as given by equation (6)

$$\textbf{Relative Phase}(\delta) = \tan^{-1}\left(\frac{-S3}{S2}\right) \quad (4)$$

The negative sign of S3 in the relative phase calculation is consistent with left circular transmission (Raney etal.,2011)

5.2.4 Poincare ellipticity (χ)

Poincare ellipticity (χ) parameter is a shape parameter which describes the degree to which the polarization ellipse is oval. The shape of the ellipse is governed by the magnitudes and relative phase between the horizontal and vertical components of the Electric Field vector (Kausika, 2008). It is an important parameter used in m-χ decompositions technique that is used to understand the dominant scattering mechanism associated with a target on the lunar surface. The Poincare ellipticity (χ)

can be calcualated by the following formulation as given by equation (8)

$$\sin 2\chi = \left(\frac{-S3}{m\,X\,S0}\right) \quad (8)$$

5.2.5 m-χ decompositions technique-

Decomposition techniques help in interpreting the scattering information embedded in the polarization of a backscattered wave. In the m-χ decomposition method m, ellipticity parameter and orientation angle were used as the three parameters for the decomposition. This method proved to be useful in characterizing the lunar double bounce backscatter from surface scattering. Hence the m– χ decomposition method was used in the present study to understand the dominant scattering mechanism associated with a target on the lunar surface. In this decomposition, the degree of circularity is given by equation (5) and the m– χ decomposition colour - coding (Raney, et al., 2012b) is given by

$$Red(R) = \sqrt{\left(\frac{S0\,X\,m\,X\,(1+\sin 2\chi}{2}\right)} \quad (9)$$

$$Green(G) = \sqrt{(S0(1-m))} \quad (10)$$

$$Blue(B) = \sqrt{\left(\frac{S0\,X\,m\,X\,(1-\sin 2\chi}{2}\right)} \quad (11)$$

Where Red colour in the output indicates the double bounce backscatter (Dihedrals reflectors), Green colour in the output indicates Volume Scattering (randomly polarized constituent) and Blue colour in the output indicates Single bounce backscatter (Bragg Scattering). By using equation (6), (7) and (8) here, the total backscattered power can be calculated, by-

$$Total\ Backscattered\ power = R^2 + G^2 + B^2 \quad (12)$$

5.3 Results

5.3.1 Byrgius Crater- In Byrgius Crater the high backscattered power is indicate by white colour while the low backscattered power is indicated by black colour as seen in Figure 13 (A). The Value

of CPR in Byrgius crater varies from 0.621- 1.045. The high value of CPR is indicated by green colour while the low value is indicated by red colour as seen in Figure 13 (B). To understand the dominant scattering the m– χ decomposition method is used as seen in figure 13 (C), corresponding colour in scale represents Double bounce scattering, surface scattering and volume scattering.

5.3.2 King Crater – In King Crate the colour coding for total backscattered power is same as that of Byrgius Crater. The total backscattered power for king crater is shown seen in Figure 14 (A). The Value of CPR in King Crater varies from -0.600- 1.246. The high value of CPR is indicated by green colour while the low value is indicated by red colour as seen in Figure 14 (B).

To understand the dominant scattering the m– χ decomposition method is used as seen in figure 14 (C), corresponding colour in scale represents Double bounce scattering, surface scattering and volume scattering.

5.3.3Taylor Crater- In Taylor Crater the colour coding for total backscattered power is same as that of King Crater. The total backscattered power for Taylor crater is shown seen in Figure 15 (A). The Value of CPR in Taylor crater varies from 0.807- 1.02. The high value of CPR is indicated by blue colour while the low value is indicated by red colour as seen in Figure 15 (B). To understand the dominant scattering the m– χ decomposition method is used as seen in figure 15 (C), corresponding colour in scale represents Double bounce scattering, surface scattering and volume scattering.

5.3.4Descartes Crater- In Descartes Crater the colour coding for total backscattered power is same as that of Taylor Crater. The total backscattered power for Taylor crater is shown seen in Figure 16 (A). The Value of CPR in Taylor crater varies from 0.048- 1.017. The high value of CPR is indicated by blue

colour while the low value is indicated by black colour as seen in Figure 16 (B). To understand the dominant scattering the m– χ decomposition method is used as seen in figure 16 (C), corresponding colour in scale represents Double bounce scattering, surface scattering and volume scattering.

5.3.5 Maunder Crater- In Descartes Crater the colour coding for total backscattered power is same as that of Taylor Crater. The total backscattered power for Taylor crater is shown seen in Figure 17 (A). The Value of CPR in Taylor crater varies from 0.048- 1.017. The high value of CPR is indicated by blue colour while the low value is indicated by black colour as seen in Figure 17(B).

To understand the dominant scattering the m– χ decomposition method is used as seen in figure 17 (C), corresponding colour in scale represents Double bounce scattering, surface scattering and volume scattering.

6. Conclusion

The present work is a summary of results from Moon Mineralogical Mapper and Mini-SAR data by Chandrayaan-1 mission. The study has brought out a methodology for Moon Mineralogical Mapper and Mini-SAR data analysis. The various outputs generated using M^3 and Mini-SAR for the given study area.

- The band shape algorithms such as standard band ratio are employed to capture compositional variation in the area.
- In King Crater Immature highland lithology is showing the absorption feature nearly 2860 nm and the CPR >1, indicating presence of water/ice molecules on the crater.
- Byrgius Crater showing absorption feature nearly 930 nm, 1390nm and 1940 nm indicating Ortho pyroxene and plagioclase composition and broad absorption at 970nm and 2060 nm indicate the high calcic pyroxene i.e. Gabbro.
- Maunder Crater showing a broad absorption feature nearly 970 nm and 2177 nm indicating pyroxene while the blue colour in standard band ratio image is showing a broad absorption at 790nm and 1489 nm indicating crystalline plagioclase.
- Taylor Crater showing absorptions feature nearly at 850 nm and 1938

nm which is indicating the high calcic pyroxene i.e. Norite and broad absorptions at 990 nm, and 1740 nm indicate the presence of high calcic pyroxene i.e. Gabbro.

- Descartes Crater showing absorption feature nearly at 910 nm and 1820 nm indicating Ortho pyroxene i.e. norite and showing broad absorption at 1008 nm and 1805 nm indicate the high calcic pyroxene i.e. Gabbro.
- 1µm and 2 µm band depths used to found the Olivine and Pyroxene mineral abundances.
- m-χ decomposition techniques help in identifying crater morphology and understanding CPR values over lunar surface.
- Derived Stokes parameters like CPR, m and χ are effective in characterizing radar scattering associated with lunar surface and subsurface features.
- Many of the features in Crater were characterized by low CPR and high backscatter values suggesting the abundance of fresh ejecta deposits with finer texture.

7. References-

1. **Arivazhagan S. and Anabazhagan S.** Lithological Discrimination of Apollo 17 Landing Site using Chandrayaan-1 Moon Minearlogical Mapper Data [Journal]. - [s.l.] : 43rd Lunar and Planetary Science Conference, 2012.
2. **Carter Lynn M., Campbell Donald B. and Campbell Bruce A.** Geologic studies of planetary surfaces using radar polarimetric imaging [Journal]. - [s.l.] : IEEE, February 10, 2011. - 5 : Vol. 99.
3. **Fa W. and Cai Y.** Analysis of CPR characteristics for anomalous crater sand implications for lunar ice detection [Journal]. - [s.l.] : 44th Lunar and Planetary Science Conference, 2013.
4. **Goswami J. N. and Annadurai M.** Chandrayaan-1: India's first planetary science mission to the Moon. [Journal]. - [s.l.] : 40th Lunar and Planetary Science Conference, 2009.
5. **Isaacson Peter J. [et al.]** The lunar rock and mineral characterization consortium: Deconstruction and integrated mineralogical, petrologic, and spectroscopic analyses of mare basalts, Meteorit [Journal]. - [s.l.] : Planet Sciences, 46. - pp. 228-251.

6. **Kausika Bhavya** POLARIMETRIC MODELING OF LUNAR SURFACE FOR SCATTERING INFORMATION RETRIEVAL USING MINI-SAR DATA OF CHANDRAYAAN-1 [Journal]. - [s.l.] : M.sc. Thesis, University of Twente, Jan 29, 2008.

7. **Mustard John F. [et al.]** Compositional diversity and geologic insights of the Aristarchus crater from Moon Mineralogy Mapper data [Journal]. - [s.l.] : Journal of Geophysical Research: Planets, June 2011. - E6 : Vol. 116.

8. **Kramer G.Y and Combe J.Ph.** THE FATE OF HYDROXYL AND WATER ON THE LUNAR SURFACE OVER TIME [Journal]. - [s.l.] : 47th Lunar and Planetary Science Conference, 2016.

9. **Mohan Shiv, Das Anup and Chakraborty Manab** Studies of polarimetric properties of lunar surface using Mini-SAR data [Journal]. - [s.l.] : Current Science, 2011. - 2 : Vol. 101. - pp. 159-164.

10. **Nozette Stewart [et al.]** Integration of lunar polar remote-sensing data sets: Evidence for ice at the lunar south pole [Journal]. - [s.l.] : Journal of Geophysical Research : Planets, October 25, 2001. - E10 : Vol. 106. - pp. 23253–23266.

11. **Pieters C. M.** Character and distribution of OH/H20 on the surface of the Moon seen by M3 on Chandrayaan-1 [Journal] // Science. - 2009b. - pp. 568-572.

12. **Raney R.K. [et al.]** The m-chi decomposition of hybrid dual-polarimetric radar data with application to lunar craters [Journal]. - [s.l.] : Journal of Geophysical Research, 2012b. - E00H21 : Vol. 117.

13. **Raney R.K.** Hybrid-Polarity SAR Architecture [Journal]. - [s.l.] : IEEE Transactions on Geoscience and Remote Sensing, Nov. 2007. - 11 : Vol. 45.

14. **Saran Sriram [et al.]** Study of scattering characteristics of lunar equatorial region using Chandrayaan-1 Mini-SAR polarimetric data [Journal]. - [s.l.] : Planetary and Space Science 71, 2012. - pp. 18-20.

15. **Spudis Paul D., Martin Dayl J. P. and Kramer Georgiana** Geology and composition of the Orientale Basin impact melt sheet [Journal]. - [s.l.] : Journal of Geophysical

Research: Planets, Januaury 2014. - 1 : Vol. 119. - pp. 19-29.

16. **V. Siva Kumar, R. Neelakantan and M. Santosh** Lunar Surface mineralogy using hyperspectral data:Implication for primordial crust in the Earth- Moon syste. [Journal] // Geoscience Frontiers. - 2017. - pp. 457-465.

Figures

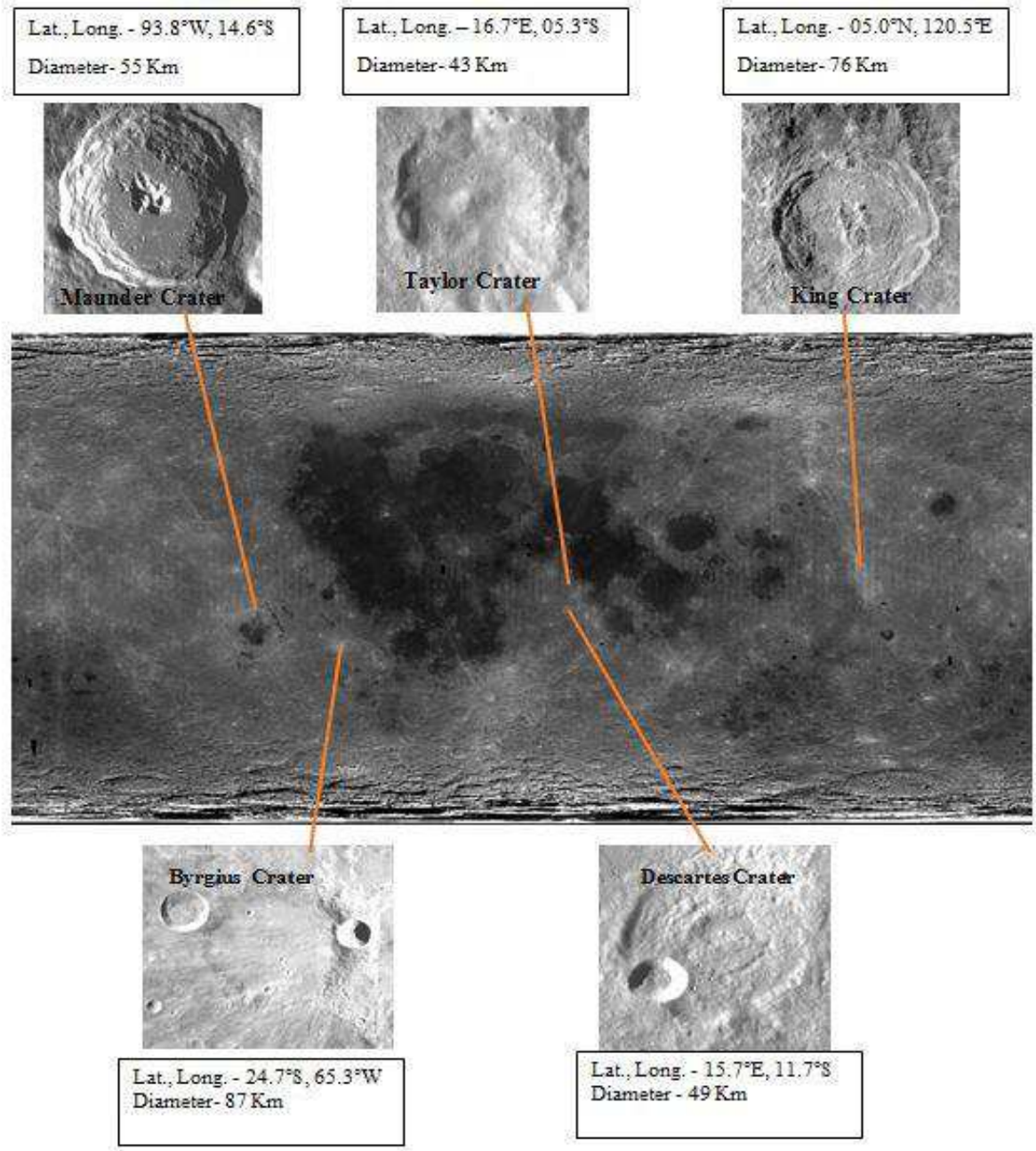

Figure 1: - The study area of craters on Lunar map. The location corresponds to the centre of the feature.

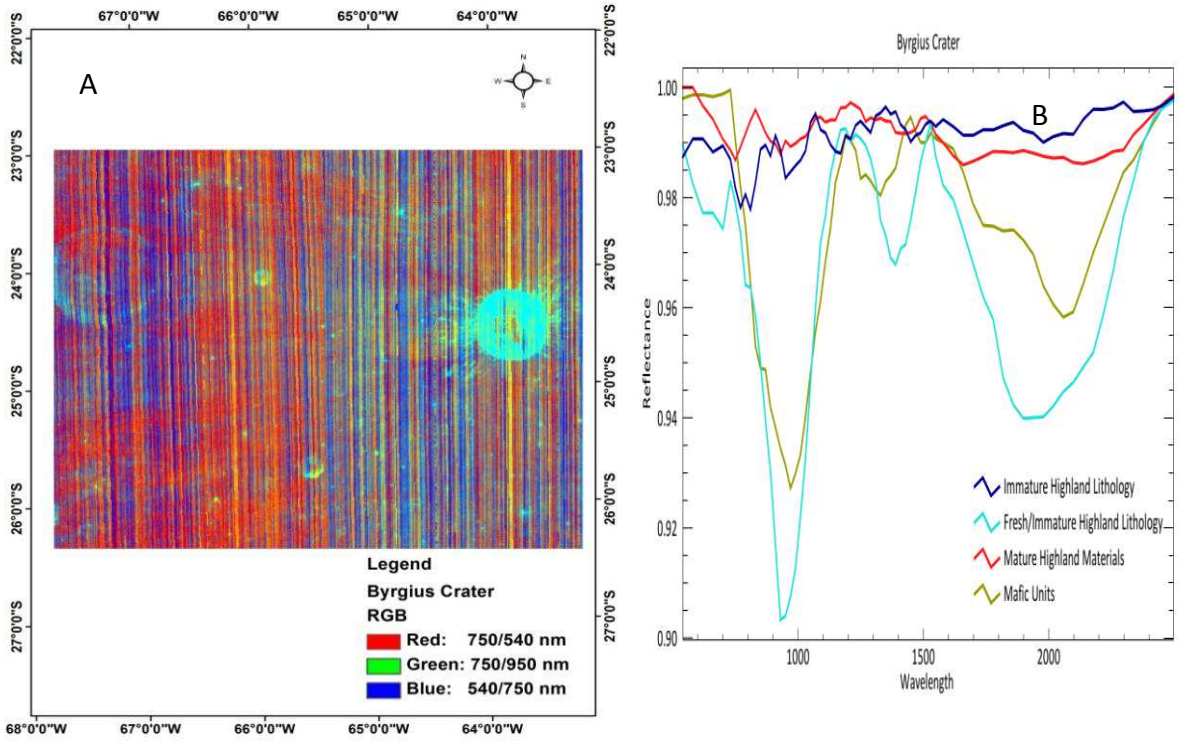

Figure 2: The Standard band ratio of Byrgius Crater (A) and continuum removed spectra of Byrgius Crater (B).

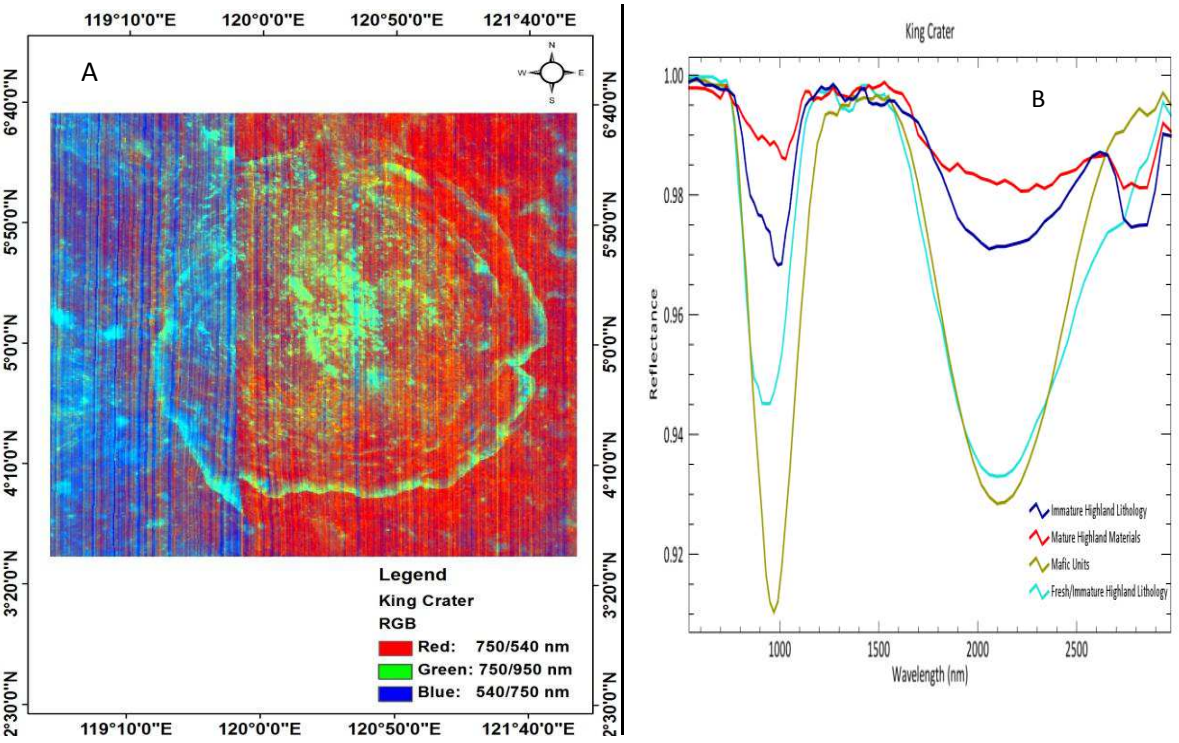

Figure 3: The Standard band ratio of King Crater (A) and continuum removed spectra of King Crater (B).

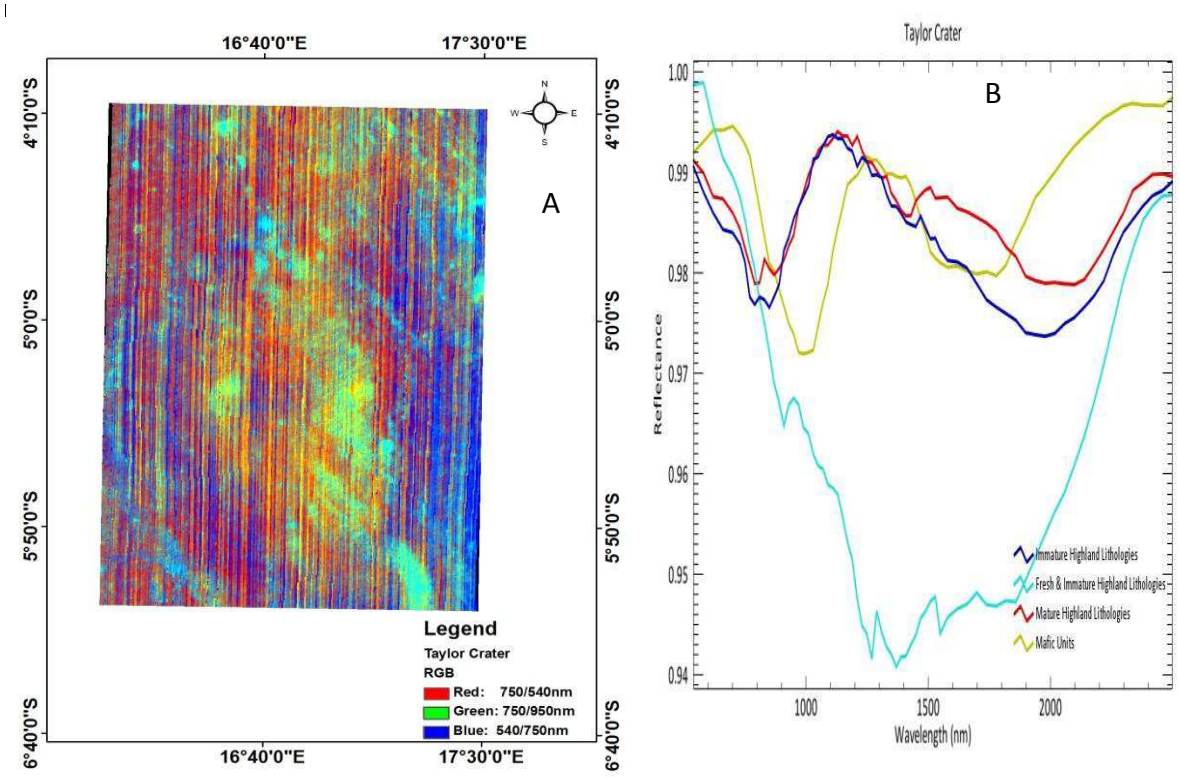

Figure 4: The Standard band ratio of Taylor Crater (A) and continuum removed spectra of Taylor Crater (B).

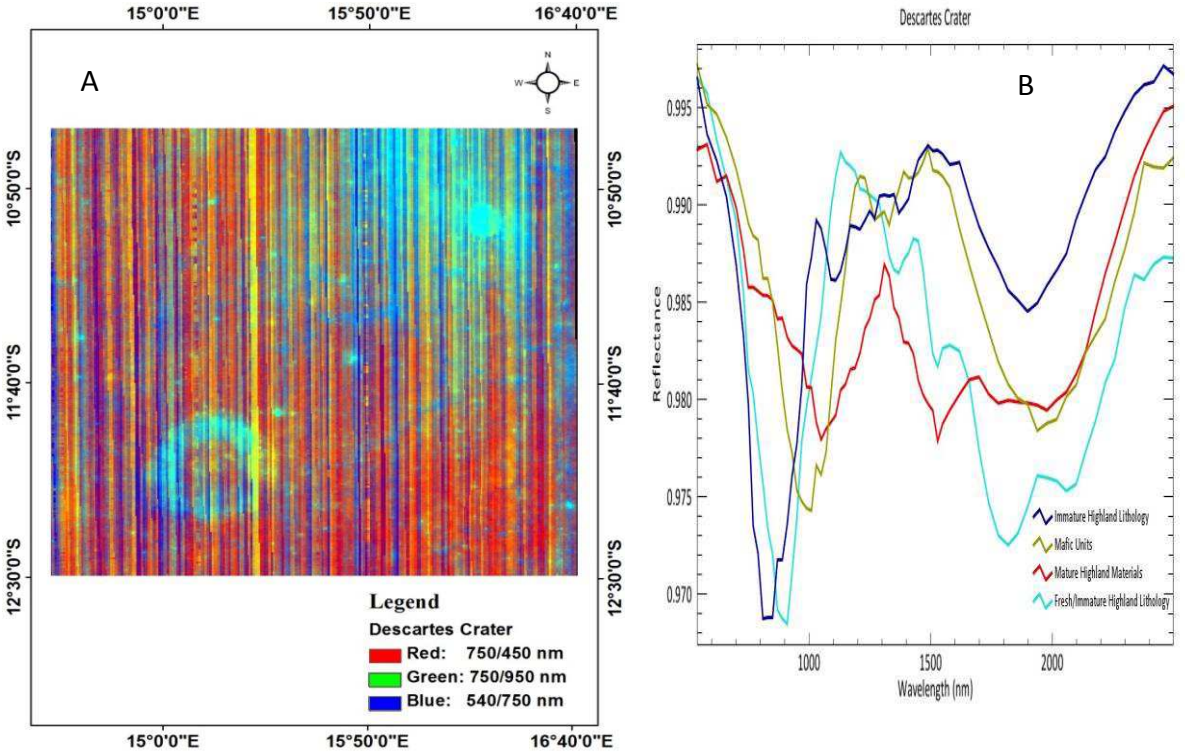

Figure 5: The Standard band ratio of Descartes Crater (A) and continuum removed spectra of Descartes Crater (B).

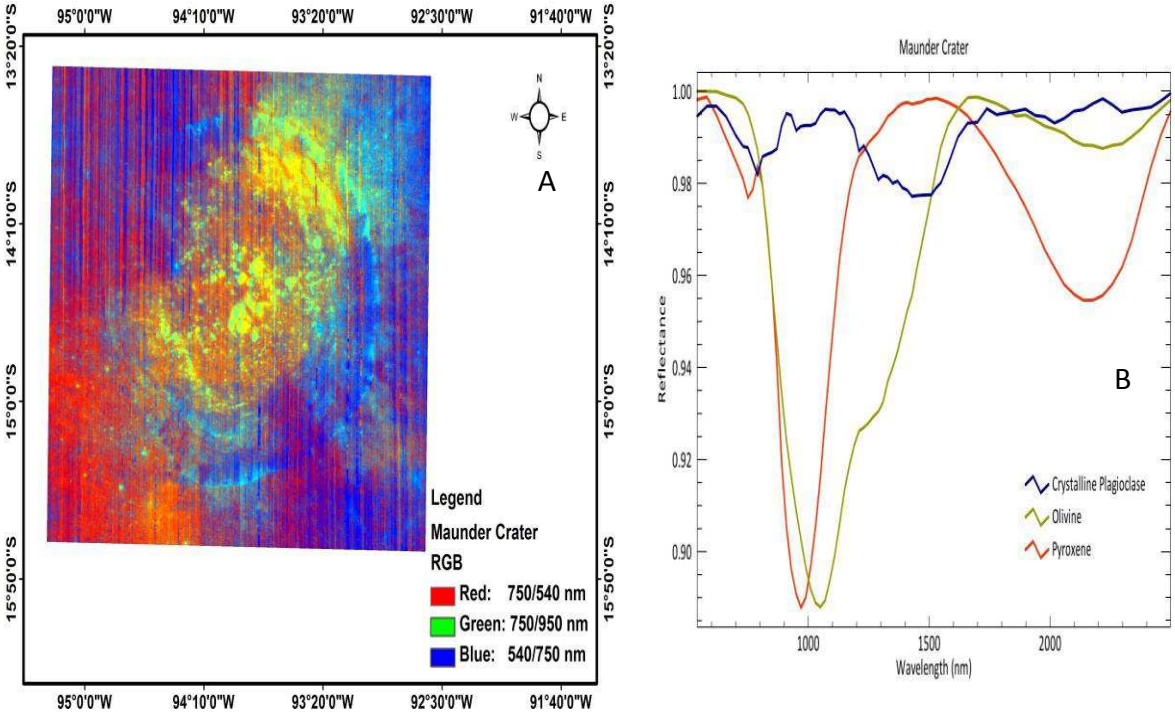

Figure 6: The Standard band ratio of Maunder Crater (A) and continuum removed spectra of Maunder Crater (B).

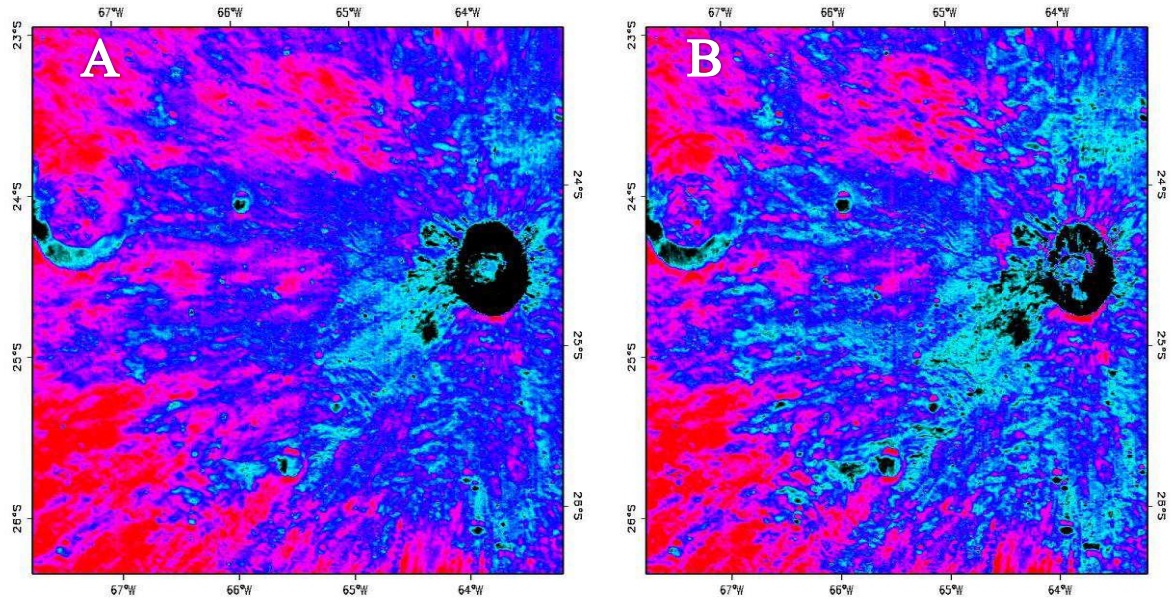

Figure 7: The 1µm band depth of Byrgius Crater (B) The 2 µm band depth of Byrgius Crater.

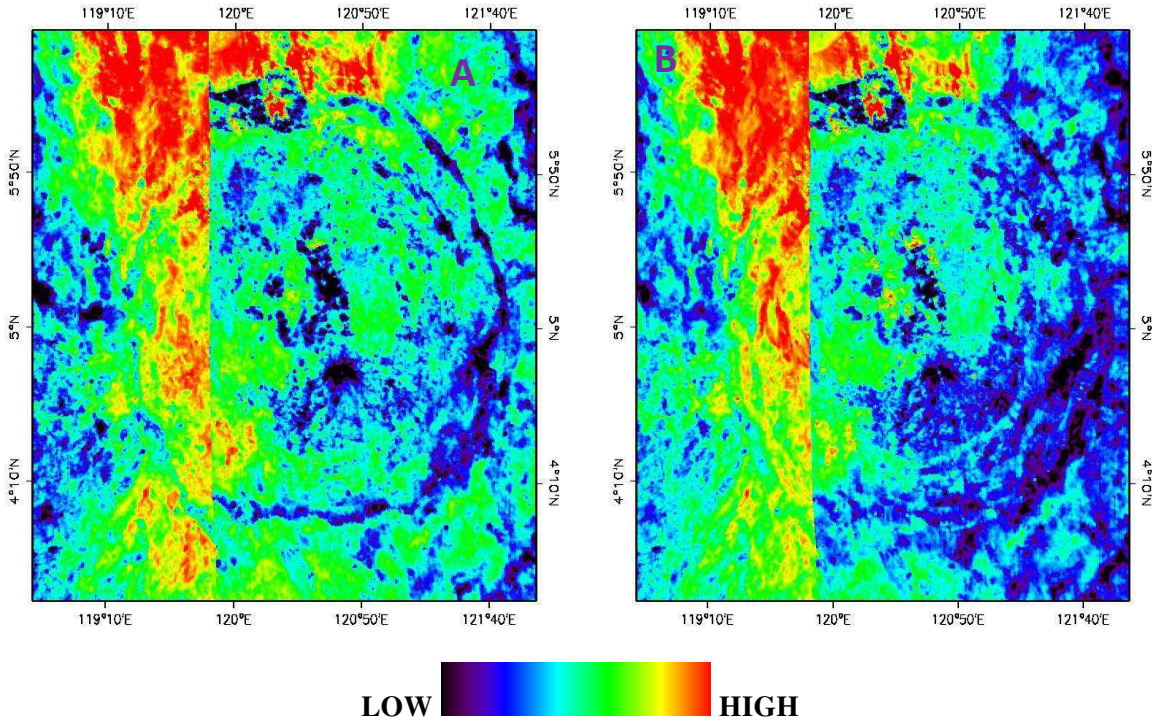

Figure 8: (A) The 1µm band depth of King Crater (B) The 2 µm band depth of King Crater .

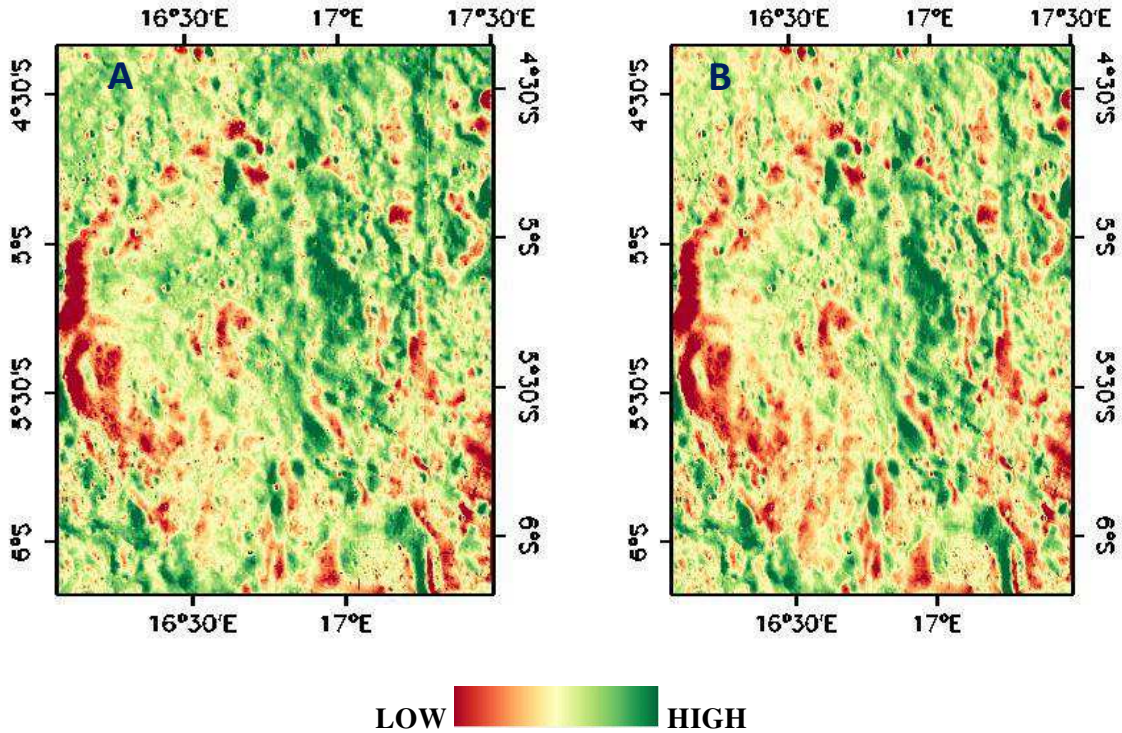

Figure 9: (A) The 1µm band depth of Taylor Crater (B) The 2 µm band depth of Taylor Crater .

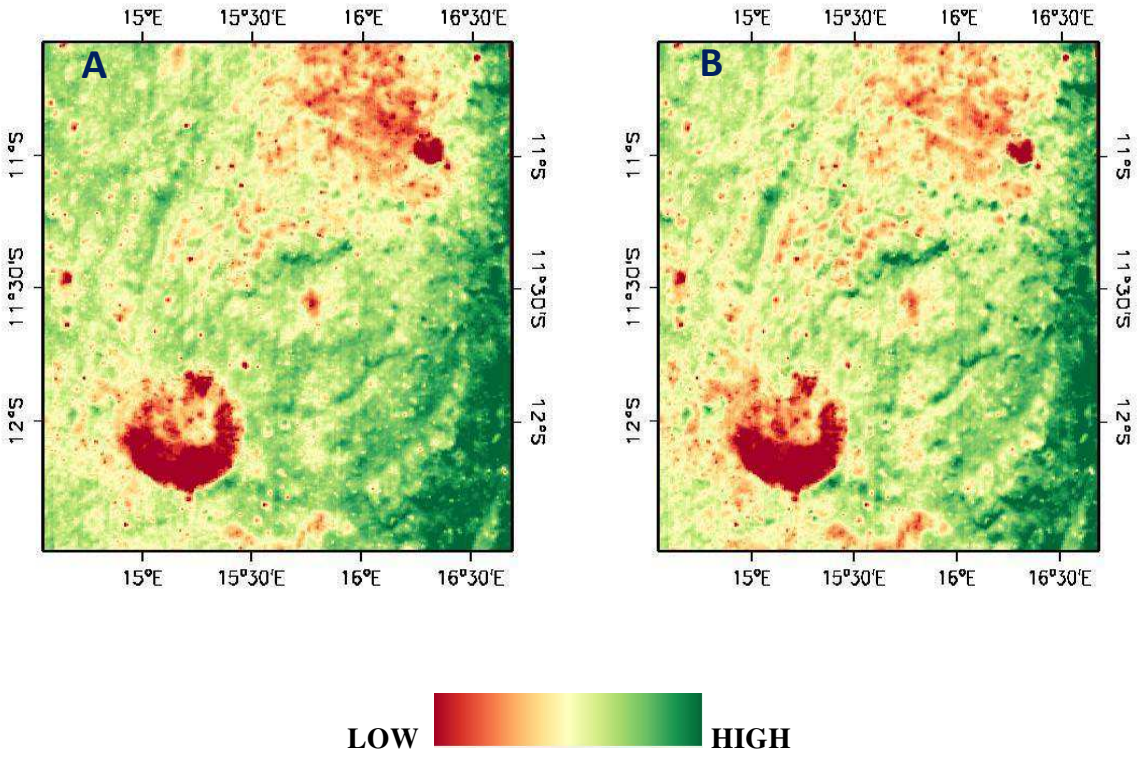

Figure 10: (A) The 1µm band depth Descartes Crater (B) The 2 µm band depth Descartes Crater.

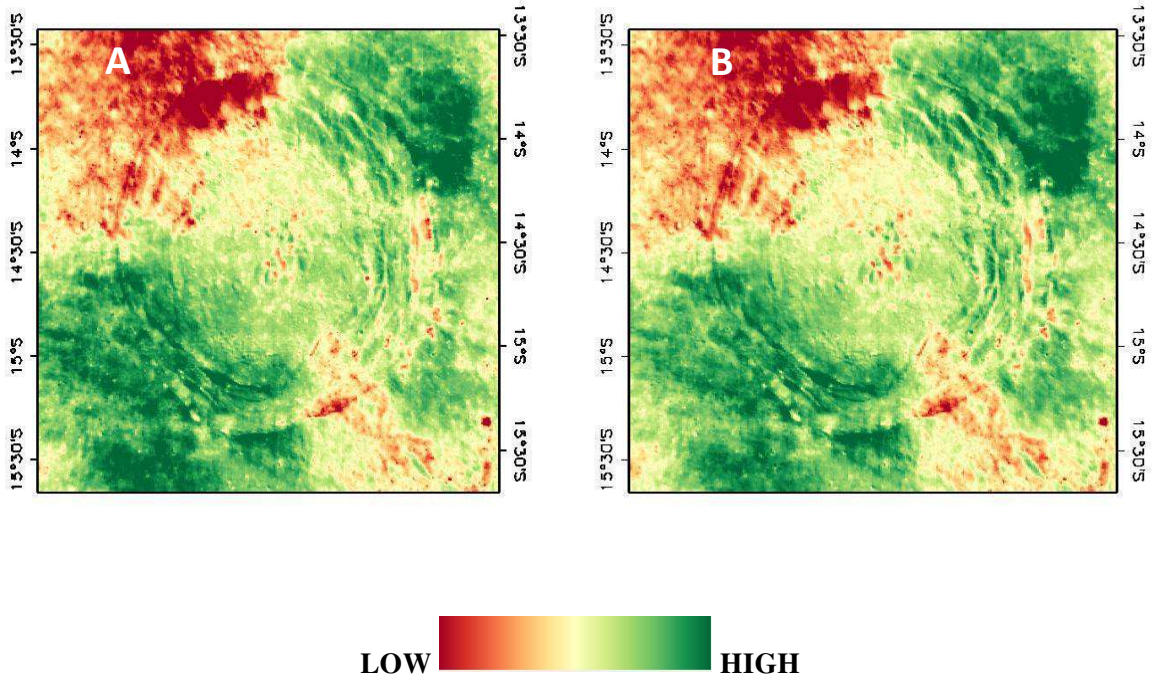

Figure 11: (A) The 1µm band depth Maunder Crater (B) The 2 µm band depth Maunder Crater.

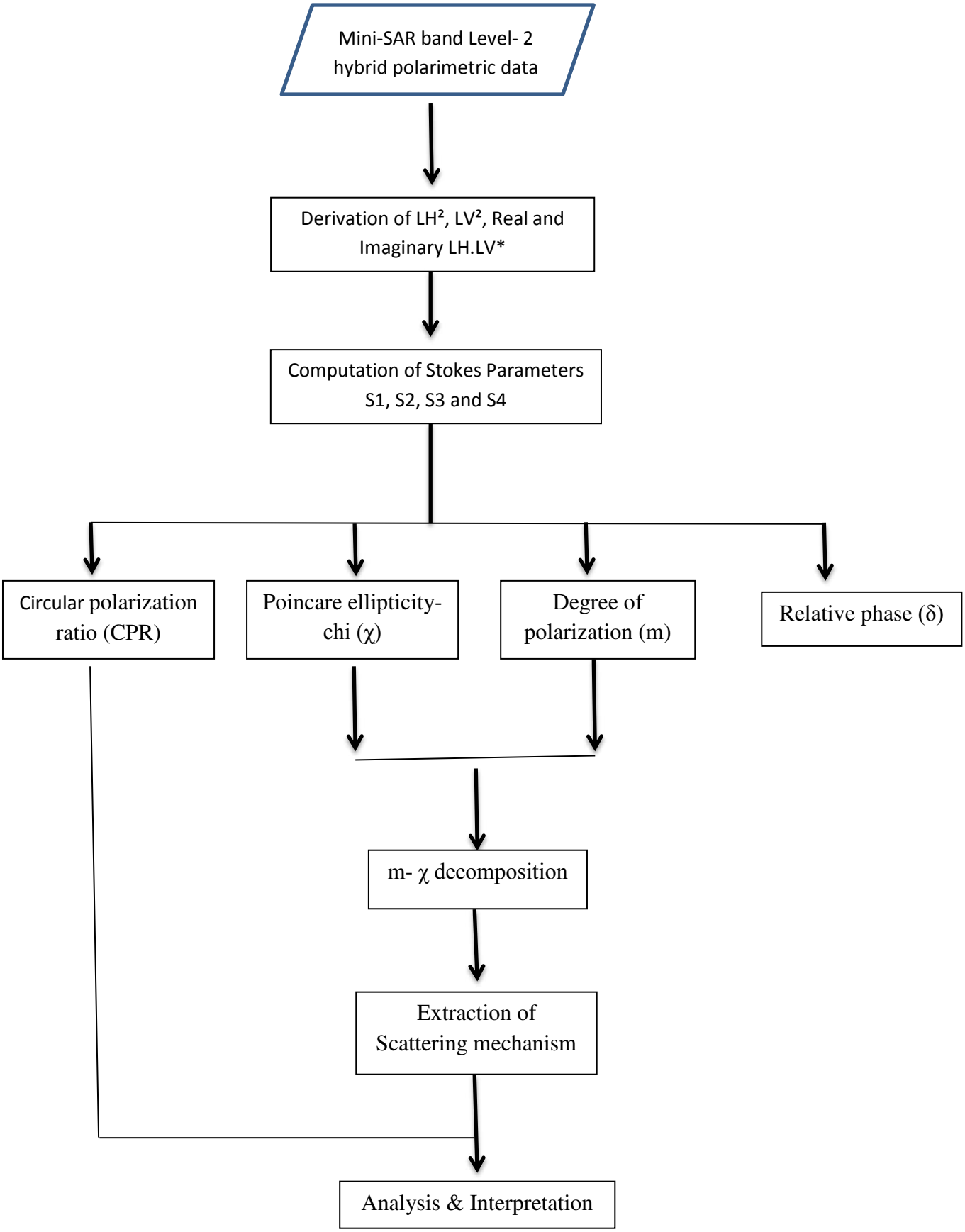

Figure 12- Methodology adopted in the present study.

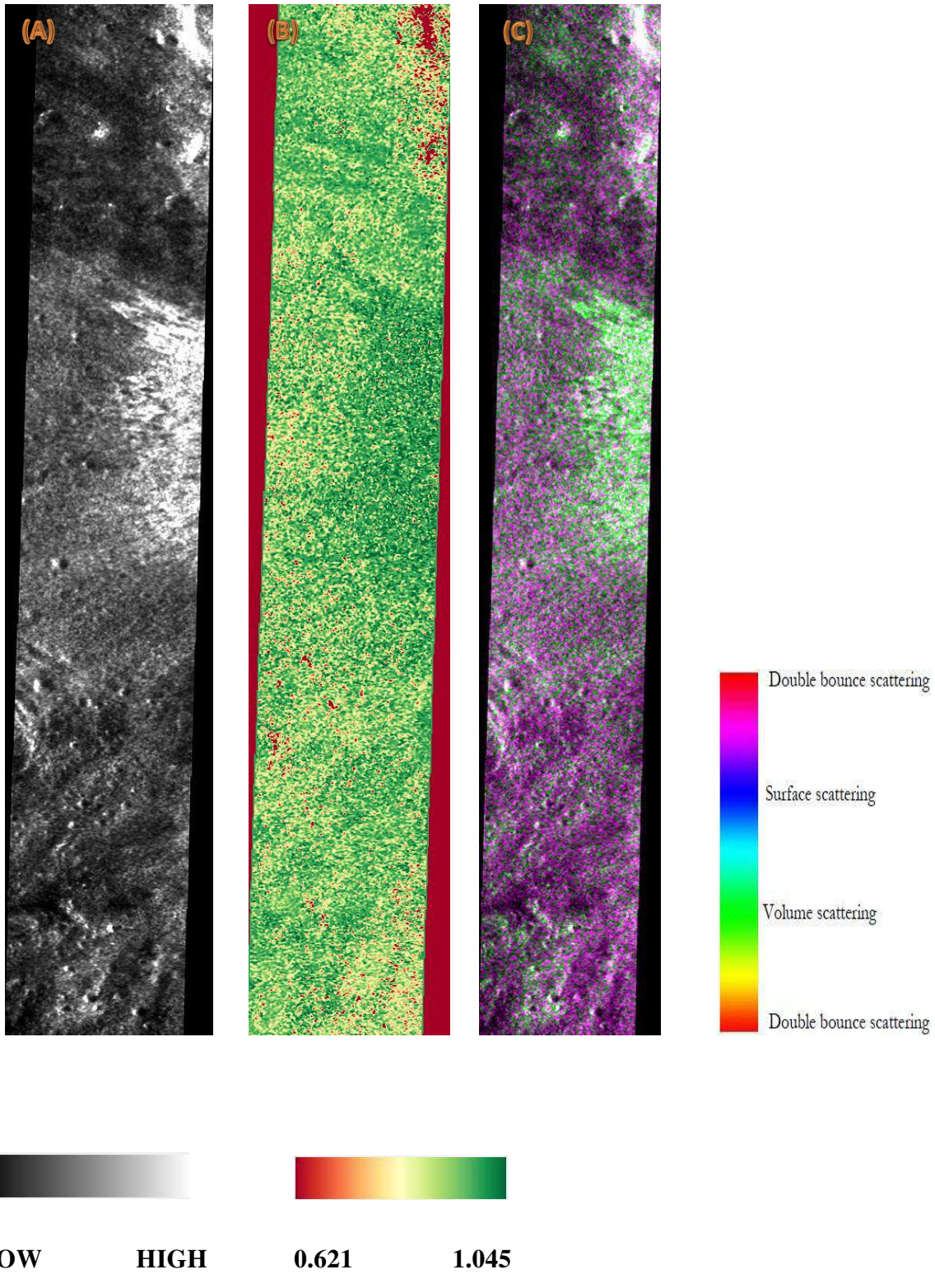

Figure 13- Byrgius crater as seen by the Mini-SAR in (a) Total back scattered power, (b) Circular polarization ratio and (c) m– χ decomposition.

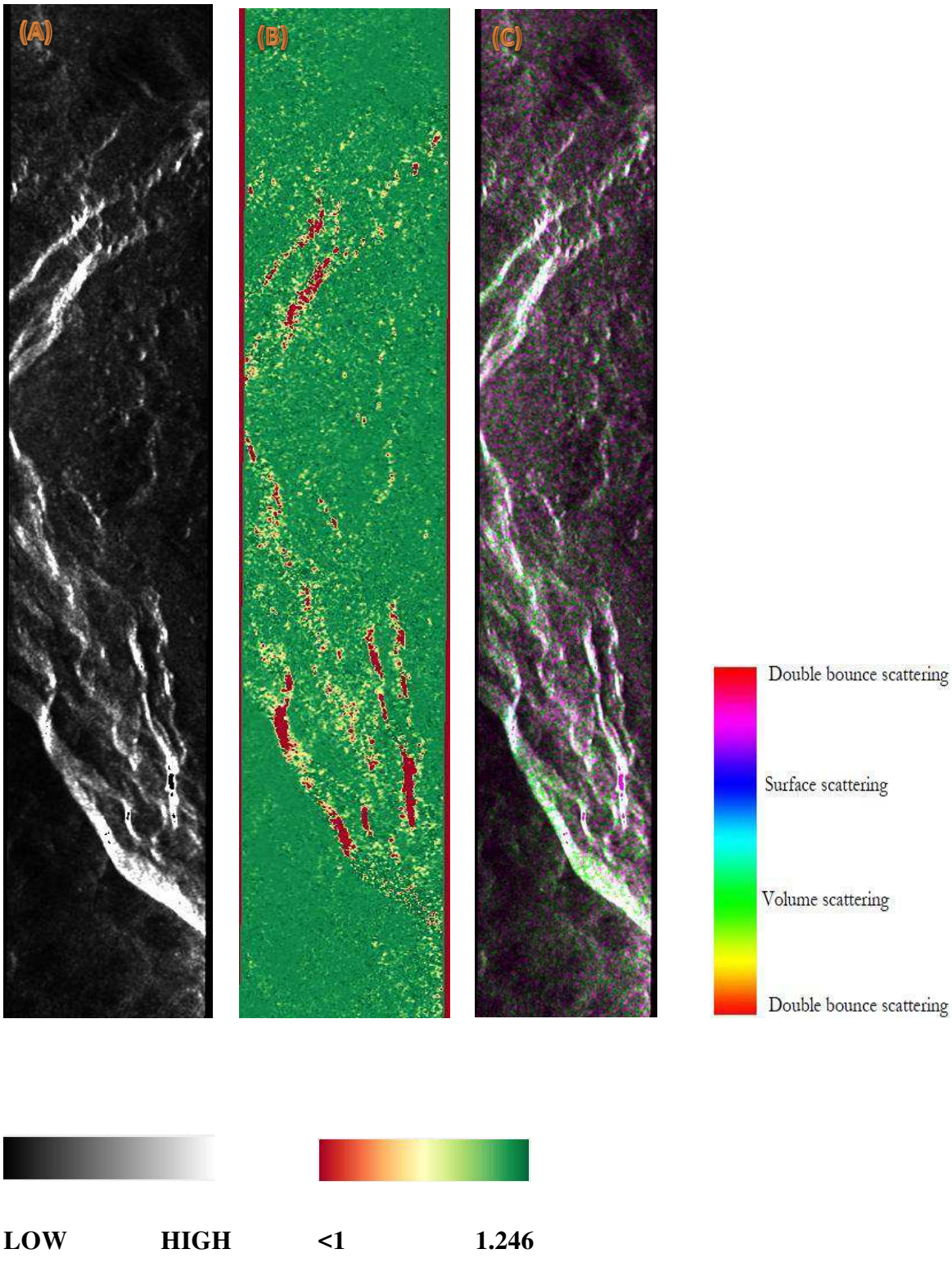

Figure 14- King Crater as seen by the Mini-SAR in (a) Total back scattered power, (b) Circular polarization ratio and (c) m– χ decomposition.

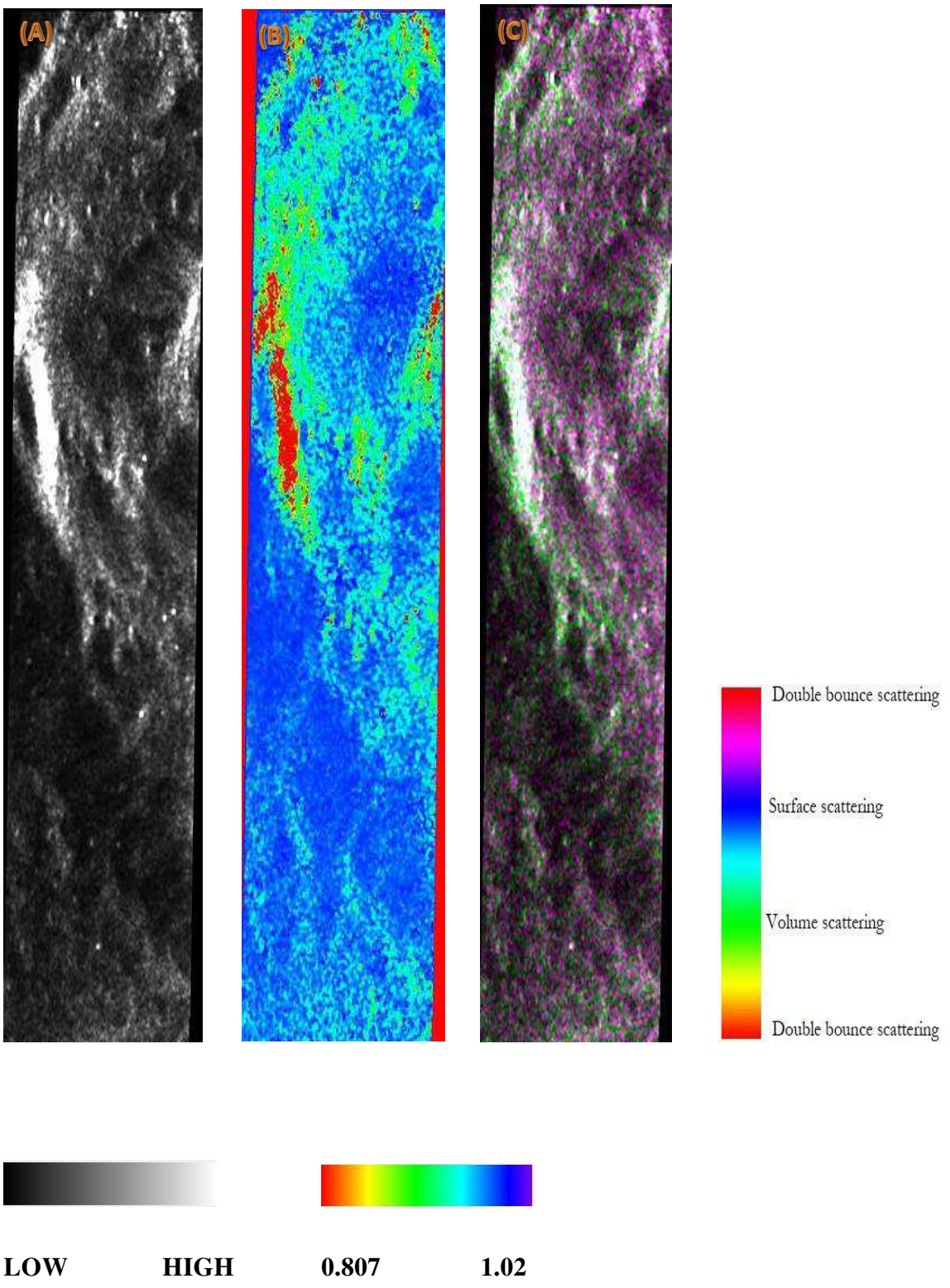

Figure 15- Taylor crater as seen by the Mini-SAR in (a) Total back scattered power, (b) Circular polarization ratio and (c) m– χ decomposition.

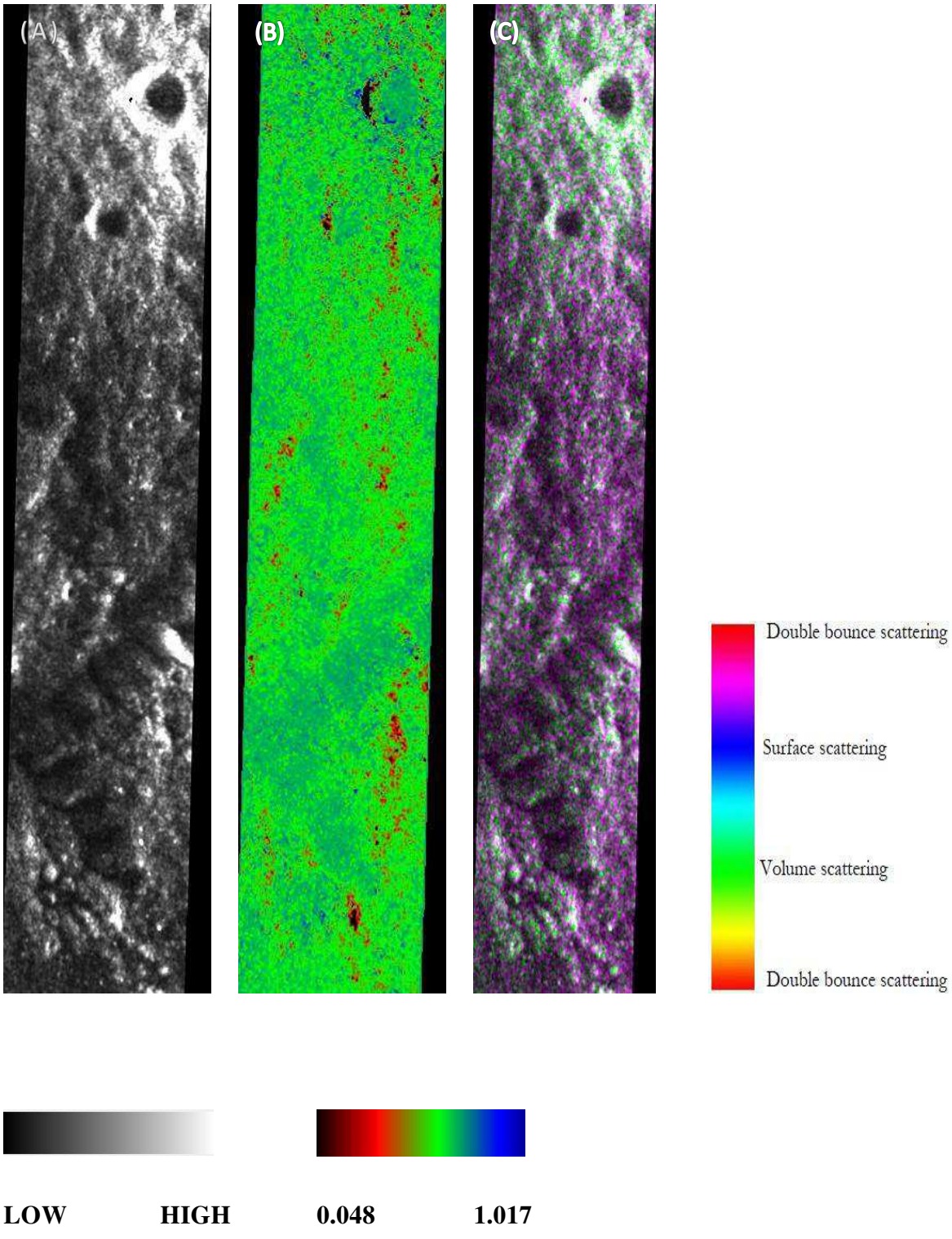

Figure 16- Descartes crater as seen by the Mini-SAR in (a) Total back scattered power, (b) Circular polarization ratio and (c) m– χ decomposition.

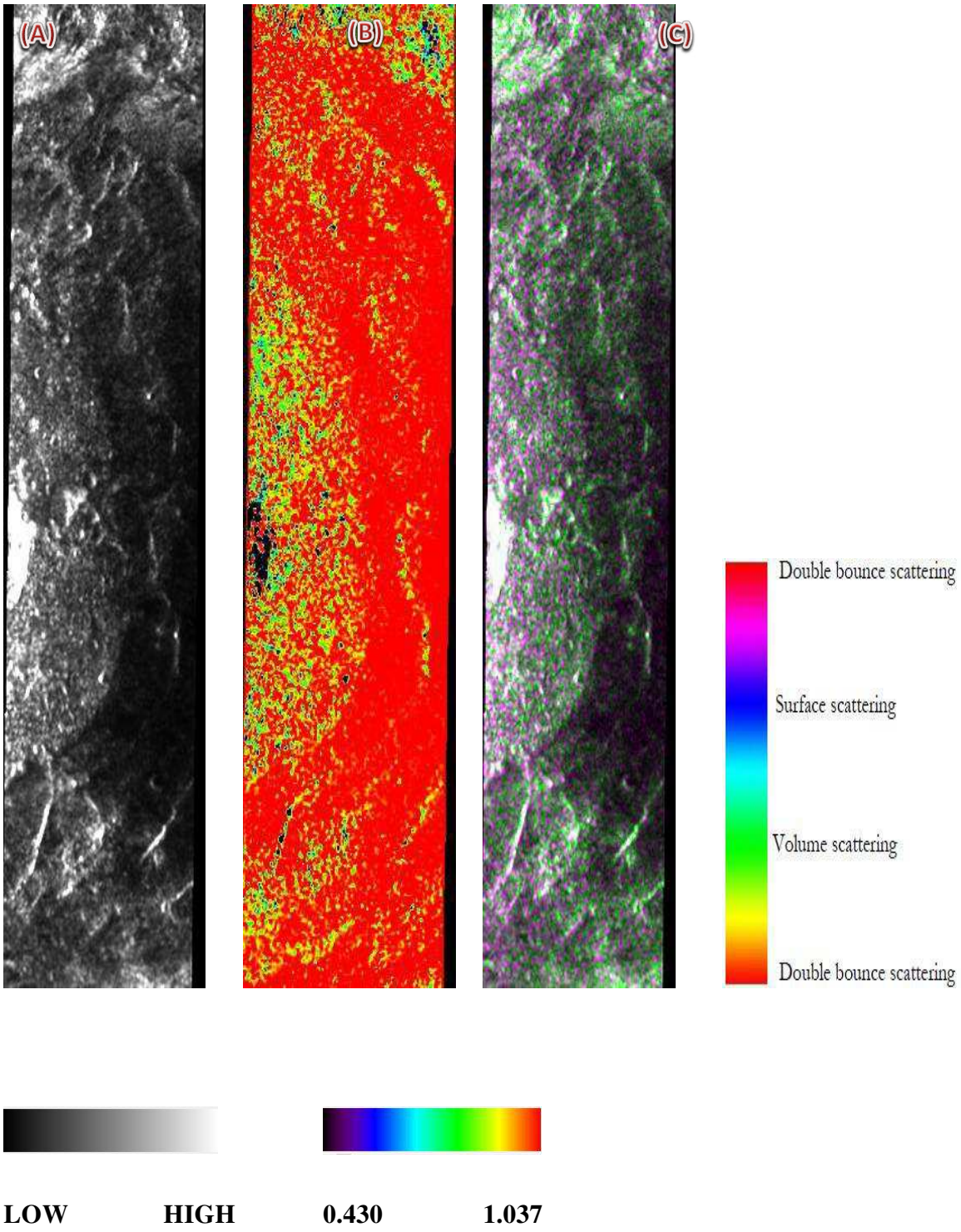

Figure 17- Maunder crater as seen by the Mini-SAR in (a) Total back scattered power, (b) Circular polarization ratio and (c) m– χ decomposition.